

Journal of Materials Chemistry A

Accepted Manuscript



This is an *Accepted Manuscript*, which has been through the Royal Society of Chemistry peer review process and has been accepted for publication.

Accepted Manuscripts are published online shortly after acceptance, before technical editing, formatting and proof reading. Using this free service, authors can make their results available to the community, in citable form, before we publish the edited article. We will replace this *Accepted Manuscript* with the edited and formatted *Advance Article* as soon as it is available.

You can find more information about *Accepted Manuscripts* in the [Information for Authors](#).

Please note that technical editing may introduce minor changes to the text and/or graphics, which may alter content. The journal's standard [Terms & Conditions](#) and the [Ethical guidelines](#) still apply. In no event shall the Royal Society of Chemistry be held responsible for any errors or omissions in this *Accepted Manuscript* or any consequences arising from the use of any information it contains.

Multiformity and fluctuation of Cu ordering in Cu₂Se thermoelectric materials

Ping Lu^{a,b,c}, Huili Liu^{a,c}, Xun Yuan^{a,c}, Fangfang Xu^{*,a,b}, Xun
Shi^{*,a}, Kunpeng Zhao^{a,c}, Wujie Qiu^a, Wenqing Zhang^a,
Lidong Chen^a

^a State Key Laboratory of High Performance Ceramics and Superfine Microstructures, and

^b Analysis and Testing Center for Inorganic Materials, Shanghai Institute of Ceramics, Chinese Academy of Sciences (CAS), 1295 Dingxi Road, Shanghai 200050, China

^c University of Chinese Academy of Sciences, 19 Yuquan Road, Beijing 100049, China

Abstract

Cuprous selenide (Cu₂Se) has recently been shown a very high dimensionless thermoelectric figure of merit zT as well as a dramatic increase in thermoelectric performance during the critical second-order phase transition. The present study indicates that the ultrahigh thermoelectric performance arises from its specific structural features involving multiformity of Cu ordering and drastic structural fluctuation during phase transition. The Cu₂Se sample consists of domains of different ordered lamellar structures for Cu atoms which are coherently immersed in the long-range ordered Se pseudo-*fcc* framework. The specific self-independent binary-sublattice structures have been found to enhance the phonon scattering while still guaranteeing good carrier mobilities. Upon increasing the temperature to near the phase transition, the multiple structures undergo intense and stepwise changes including appearance of new ordered structures for copper, disordering and diffusing of Cu atoms across the interlayers, and finally random distribution of Cu in the Se cubic sublattice which has altered little during the phase transition. Such extreme structural fluctuation results in critical electron and phonon scatterings that expedite

an exceptional enhancement of thermoelectric performance.

Introduction

Since the discovery of Seebeck effects, Peltier effects and Thomson effects, thermoelectric materials have attracted widespread interest for its potentials to deal with energy crisis.^{1,2} Thermoelectric materials exploit these thermoelectric effects to realize the direct conversion between heat and electric energy, which can be applied as the power generators and air-conditioning compressors.³⁻⁶ The energy conversion efficiency is generally evaluated by the dimensionless thermoelectric figure of merit zT ($zT=S^2\sigma T/\kappa$), where S is Seebeck coefficient or thermopower, σ is electrical conductivity, T is absolute temperature, and κ is thermal conductivity.¹ Therefore, excellent thermoelectric performance (high zT value) requires high electrical transport performance but low thermal conduction, which are always mutually controversial for most materials. So far, seeking high-efficiency thermoelectric materials is still a great challenge⁷ and many strategies such as nanocrystallization^{8,9} and forming superlattices^{10,11} have been utilized to modulate the transport properties of the thermoelectric materials. Our recent study has demonstrated that cuprous chalcogenide ($\text{Cu}_{2-\delta}\text{X}$, X=S or Se)¹², especially cuprous selenide ($\text{Cu}_{2-\delta}\text{Se}$, $\delta=0\sim 0.02$), a simple binary compound, shows excellent thermoelectric performance with zT up to 1.5 at 1000 K.¹³ Meanwhile, a dramatic increase in zT by a factor of 3-7 times with a peak value of 2.3 has been observed during the critical point (at about 400 K) caused by the phase transition from room temperature α -phase to high temperature antiferrotype-type β -phase.¹⁴⁻¹⁷ These high zT values make $\text{Cu}_{2-\delta}\text{Se}$ among the best thermoelectric materials.

Despite a clear structural determination of high temperature β -phase which exhibits a face-centered cubic cell for Se atoms while Cu atoms randomly distribute at either the body-centered ($8c$) or the face-centered ($32f$) sites of Se tetrahedrons,¹⁸⁻²² the room temperature phase structure of Cu_2Se has not been explicitly clarified. A tetragonal unit cell was reported early in 1945 and an orthorhombic structure was

proposed later in 1971.²³ In 1974, Murray and Heyding worked out a monoclinic structure for Cu_2Se .²⁴ Via X-ray powder diffraction analyses of a series of copper selenides, they established a structural model for the $\text{Cu}_{1.8}\text{Se}$ phase consisting of a *fcc* sublattice of Se atoms and interstitially occupied copper atoms at either tetrahedral or trigonal sites.²⁵ Another monoclinic cell was proposed by Vucik *et al* by characterization of electron diffraction patterns.²⁶ Meanwhile, they investigated the phase transition from α -phase to β -phase of Cu_2Se , indicating that the origin of the transition was the modulation of Cu distribution along the cubic [111] direction. Later, Kashida and Akai identified the room-temperature structure of Cu_2Se as pseudo-monoclinic and characterized the structure by a periodic array of vacant tetrahedral and interstitial copper atoms, forming a ladder-like structure.²³ Nguyen *et al.* further indicated by theoretical calculation that the structures of Cu_2X (X = Te or Se) preferred a unique but unrecognized layered structure.²⁷ Our recent study confirmed the lamellar fashion of Cu_2Se room temperature phase structure by both theoretical and experimental investigations while different forms may exist⁷. The uncertainty of Cu_2Se room-temperature structures may arise from its possible multiformity which is hard to be clarified by diffractometry methods like XRD.

The mechanism behind the high thermoelectric performance in $\text{Cu}_{2-\delta}\text{Se}$ is quite interesting and special. As revealed in our previous work and further confirmed by the recent literatures,^{13,17,28,29} the very low thermal conductivity is believed to be originated from copper ion liquid-like sublattice. The cutoff of the transverse phonons at high temperatures makes $\text{Cu}_{2-\delta}\text{Se}$ display liquid-like behavior with the lowered specific heat below Dulong-Petit law and the very short phonon mean free path in the scale of atomic distances. In addition to the very low thermal conductivity at high temperatures, $\text{Cu}_{2-\delta}\text{Se}$ displays similar or even lower lattice thermal conductivity below room temperature. This is very interesting and abnormal since $\text{Cu}_{2-\delta}\text{Se}$ is a good crystalline semiconductor that usually has large thermal conductivity in this simple binary compound. Albeit low thermal conductivity, $\text{Cu}_{2-\delta}\text{Se}$ shows very good electrical conductivity, which is comparable to other typical semiconductors composed mainly of covalent bonds with good carrier mobilities. The room

temperature electrical conductivity for $\text{Cu}_{2-\delta}\text{Se}$ is higher than 10^5 S/m and the carrier mobility is between $20\text{--}40$ $\text{cm}^2\text{V}^{-1}\text{s}^{-1}$, similar to filled skutterudites³⁰. The electrical conductivity of $\text{Cu}_{2-\delta}\text{Se}$ is found to decrease a little at high temperatures. This is quite special since the liquid-like ions are expected to affect the electrical transport because the charge carriers could be strongly scattered. It seems that there could be independent transport kinetics for phonons and electrons, respectively, which may arise from the possible unusual structural features in $\text{Cu}_{2-\delta}\text{Se}$.

In this paper, we applied transmission electron microscopy (TEM) to investigate the room temperature structures and structural characteristics of Cu_2Se by taking references of the reported structures and new calculated structures in the present study. Considerable multiformity of Cu ordering in a lamellar structure has been revealed where different ordered structures bear a coherent configuration giving a specific hybrid microstructure composed of long-range ordering of Se and polymorphs of Cu ordering therein. Evolution of ordered structures examined by *in-situ* TEM in a heating process visualizes a sustained structural modulation in which more types of ordered structures appear, disappear or re-appear along with occurrence of randomness and complicity of ordering configuration. The as-revealed multiformity and fluctuation of Cu ordering in a uniform and stable Se sublattice are believed to be the structural insight for the extraordinary low thermal conductivity and moderate carrier mobility in the normal phases and during phase transitions.

Experiment

Cu_2Se samples were prepared by melting Cu (shot, 99.999%, Alfa Aesar) and Se (shot, 99.999%, Alfa Aesar) with the atomic ratio of Cu:Se=2:1 in pyrolytic boron nitride crucibles enclosed in a fused silica tube at 1423 K for 24 hours under vacuum.⁷ The melt was then cooled down very slowly to 923 K in 50 hours and was kept at this temperature for 5 days. Finally the bulk material was slowly cooled down to room temperature in 50 hours.

The as-prepared ingot was sampled in both ultra-thin foil and powder forms for

the structural characterization by field emission transmission electron microscopy (JEM-2100F, JEOL, Japan, and Tecnai-F20, FEI, USA). The powder sample was prepared by grinding the bulk materials in agate mortar and then was dispersed in ethanol by ultrasonic processing. The suspended solution was moved onto a Cu grid coated with a thin carbon film. Thin foils for TEM were polished by ion milling and were coated with a thin carbon film. *In situ* TEM observation for structural evolution was carried out using a double-tilt heating holder (Gatan Model 652). Image processing was performed using the *DigitalMicrograph* software (Gatan Inc., Pleasanton, CA, USA) and structural models were built using the *CrystalMaker* software (CrystalMaker Software Ltd, Yarnton, Oxfordshire, UK). The *MacTempas* (Total Resolution LLC, CA, USA) software was used for the simulation of electron diffraction patterns.

The thermal conductivity from 2 K to 300 K was carried out using PPMS (Quantum Design) with the TTO option under high vacuum. Before the samples were measured, the system was corrected using a standard sample of metallic nickel. The Hall resistance (R_H) and the electrical conductivity were measured using the Hall and Resistivity options for an AC transport on Quantum Design PPMS, respectively.

Results and discussions

I. Structural Characteristics and Evolution

Multiformity of Cu ordering at room temperatures

Recent theoretical and experimental analyses have verified a layered structure character of the low temperature α -Cu₂Se phases, but the exact clustering structures of Cu within the layers are still not precisely determined and remain controversial. Derived from the high temperature cubic (*fcc*, Fm-3m) β -phase, Se atoms maintain an approximate face-centered sublattice at low temperatures while Cu atoms alternately gather into a {111} interlayer of Se *fcc* sublattice, leaving interlayer empty of Cu at its

either side. Our previous first-principles calculations have predicted two types of layered α -Cu₂Se structures which have nearly the same low energies and are denoted as S1 (triclinic, SG: P-1) and S2 (monoclinic, SG: C2/c) structure, respectively (see Fig. 1).¹⁷ Here in this work, we use the same theoretical method to work out another possible triclinic structure of even lower energy (denoted as S3, and see Fig. 1 and supporting information). The energies of the three calculated phases are listed in the supporting information (see Table S2). It should be emphasized here that the indices of crystallographic directions or planes in this paper all refer to the high temperature *fcc* cubic structure (denoted with subscript “c”) for clarity, which is the parent phase structure that the room temperature structures derive from.

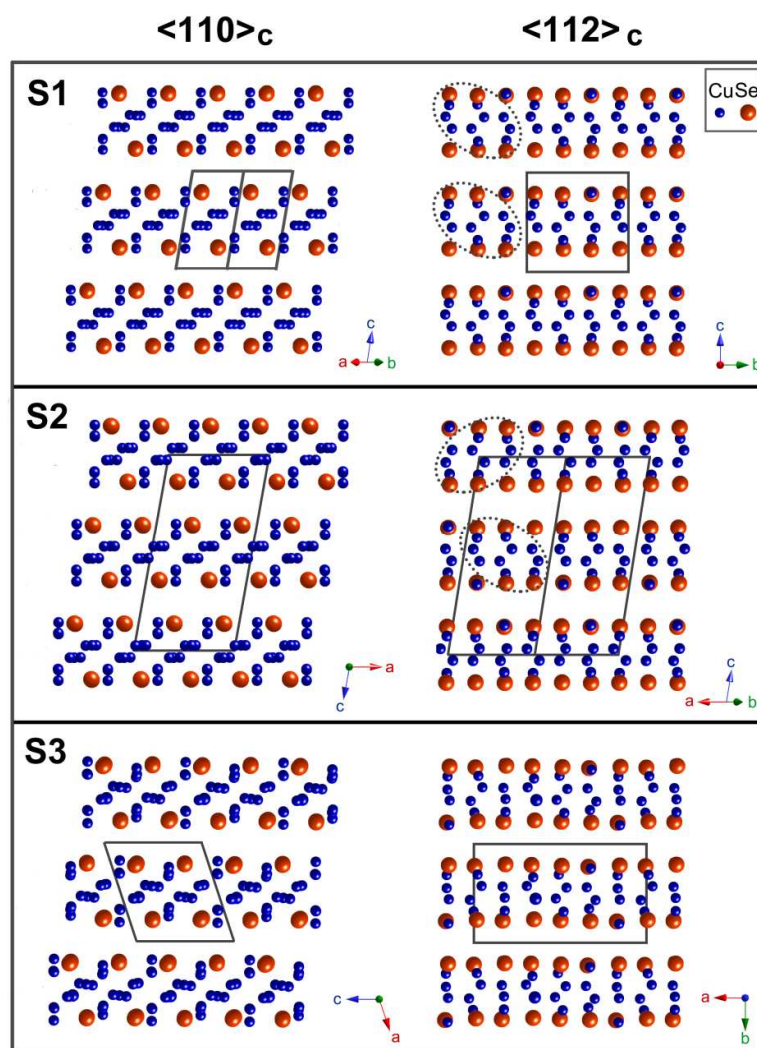


Figure 1. Structural models of three theoretically predicted room-temperature structures of Cu₂Se named as S1, S2, and S3 viewed along $\langle 110 \rangle_c$ and $\langle 112 \rangle_c$ direction, respectively.

The predicted variety of layered structures with similar low energies implies possible multiformity of room-temperature phases. Figure 2a, b and c, d illustrate the experimental and simulated diffraction patterns peculiar to S3 and S2 structure, respectively. We have not been able to obtain experimental diffraction patterns typical of S1 structure. Actually, even the diffraction patterns of pure S2 or S3 phase could not be frequently observed, while more often the patterns appear to be more complicated but still retain the layered structure character (see Fig. 2e and f, for examples). Compared to Fig. 2c, the diffraction patterns in Fig. 2e and f contain more reflections at the arrowed arrays, suggesting a large periodicity of layer stacking. Extensive TEM observation indicates that four-fold of layer packing period prevails but the reflection configuration can vary. It seems that the weak van der Waals interlayer interaction in the Cu₂Se lamellar structure could easily evoke a number of lattice translations, e.g. layer displacement, rotation around the layer normal, and mirror or glide operations. This would bring about multiformity and complicity of layered structures. The as-revealed four-fold packing superstructures are a typical example, for which a possible structural model is proposed in the supporting information (Fig. S1). Actually, more types of four-fold packing have been observed (see below), which could not be precisely clarified so far.

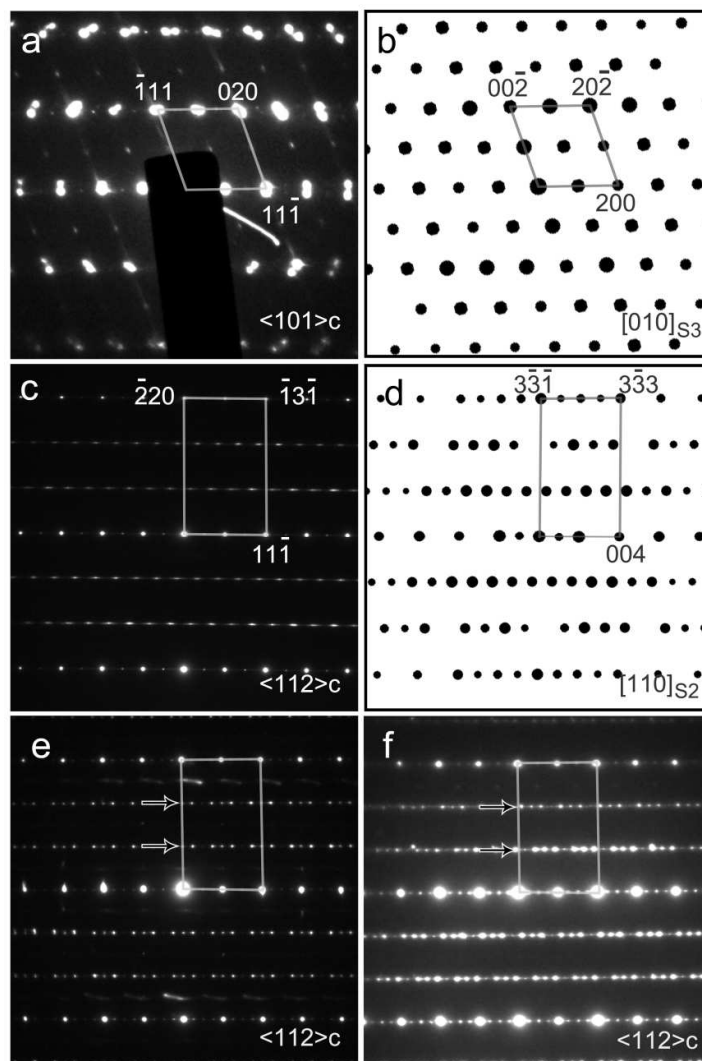


Figure 2. Experimental (dark background) and simulated (white background) diffraction patterns: (a) and (b) for S3 structure, and (c) and (d) for S2 structure. The experimental diffraction patterns ((a) and (c)) are indexed using the parent cubic lattice while the simulated diffraction patterns, for comparison, are indexed according to the predicted S3 (b) and S2 (d) structure, respectively. (e) and (f) show two examples of experimental diffraction patterns which contain more reflections at the arrowed arrays.

Despite the complicity in layer packing fashion, the arrangement of Cu atoms within each interlayer is quite similar. Our previous atom-resolved imaging has proved the proposed configuration of Cu atoms for S1 or S2 structure.⁷ Thus Cu atoms still occupy the sites in the close vicinity of trigonal or tetrahedral interstices but show an ordered distribution resulting in a planar 3×3 superlattice in S1 and S2

structures (see Fig. S2a) and $3 \times 3\sqrt{3}$ superlattice in S3 (see Fig. S2b). This is also evidenced by tripled interplanar distances for the lattices in the layer plane (referring to additional TWO rows of reflections (arrowed) on $\langle 112 \rangle_c$ projected diffraction patterns in Fig. 2e and f). Since only 40% of interstices are occupied by Cu atoms in an interlayer, there could be a variety of possible ordered structures for Cu, among which the three proposed structures exhibit low energy and then are considered to be possible room temperature structures.

Since all possible room temperature α -structures are derived and actually obtained from the high temperature cubic β -phase, the high symmetry of *fcc* cubic structure provides different ways that are equivalent to the formation of α -phases. For example, each of the four $\{111\}_c$ planes in a *fcc* unit cell may turn to be the layer plane for α -structure. Meanwhile, the trigonal symmetry of the layer plane also infers three equivalent ways for the Cu arrangement. All these configurations may occur with almost the same probability in a second-order phase transition. This implies coexistence of different ordered structures and structural orientations but with a lattice arrangement of high coherency. Figure 3 illustrates two typical examples for lattice coherency in Cu_2Se . In the first example (Fig. 3a), the layer plane is fixed on a certain $\{111\}_c$ of the parent cubic structure and is continuous across different layered structures. The diffractograms prove the perfect structural orientation where both the cubic sublattice (framed reciprocal lattice) and the layer plane are identical. The framed small region (indexed as α) refers to the S3 structure whose diffraction pattern (Fig. 3b) is peculiar along a specific $\langle 110 \rangle_c$ direction (also see Fig. 2a) while the matrix lattice could be either S1, S2 or S3 (Fig. 3c) due to their similarity along another $\langle 110 \rangle_c$ direction. In the second example (Fig. 3d), the layer planes (the left-handed region) terminate at the subgrain boundary. The diffractogram (Fig. 3f) of the right-handed region indicates the S3 structure but viewed along a $\langle 110 \rangle_c$ direction other than parallel to the layer plane. Despite the large difference in lattice structures, it can be seen that the cubic sublattice and orientation (see the framed reciprocal lattices) are substantially identical for the two parts. Therefore, the two regions have

formed room temperature layered structures on different $\{111\}_c$ planes within a single *fcc* sublattice.

Coexistence of different structures and/or orientations but in a coherent fashion results in the formation of domains (see also Fig. S3). Extensive TEM analyses confirm such specific domain texture all over the Cu_2Se ingot samples. The domain structures should be inherent from a second-order phase transition in which different ways that are equivalent in the high symmetrical high temperature structure could be applied to generate the low temperature phase structures. In Cu_2Se , Se atoms move a little during the phase transition and approximately maintain the *fcc* framework while Cu atoms diffuse a great deal within the Se sublattice in different ways. As a whole, the Cu_2Se sample shows a specific structural characteristics consisting of variety of Cu ordered structures immersed in the uniform Se cubic sublattice. Such special geometry provides pathway for electrons in a long-range crystalline framework while phonons are frequently scattered by the domain boundaries, i.e. a favorable microstructure for high thermoelectric performance.

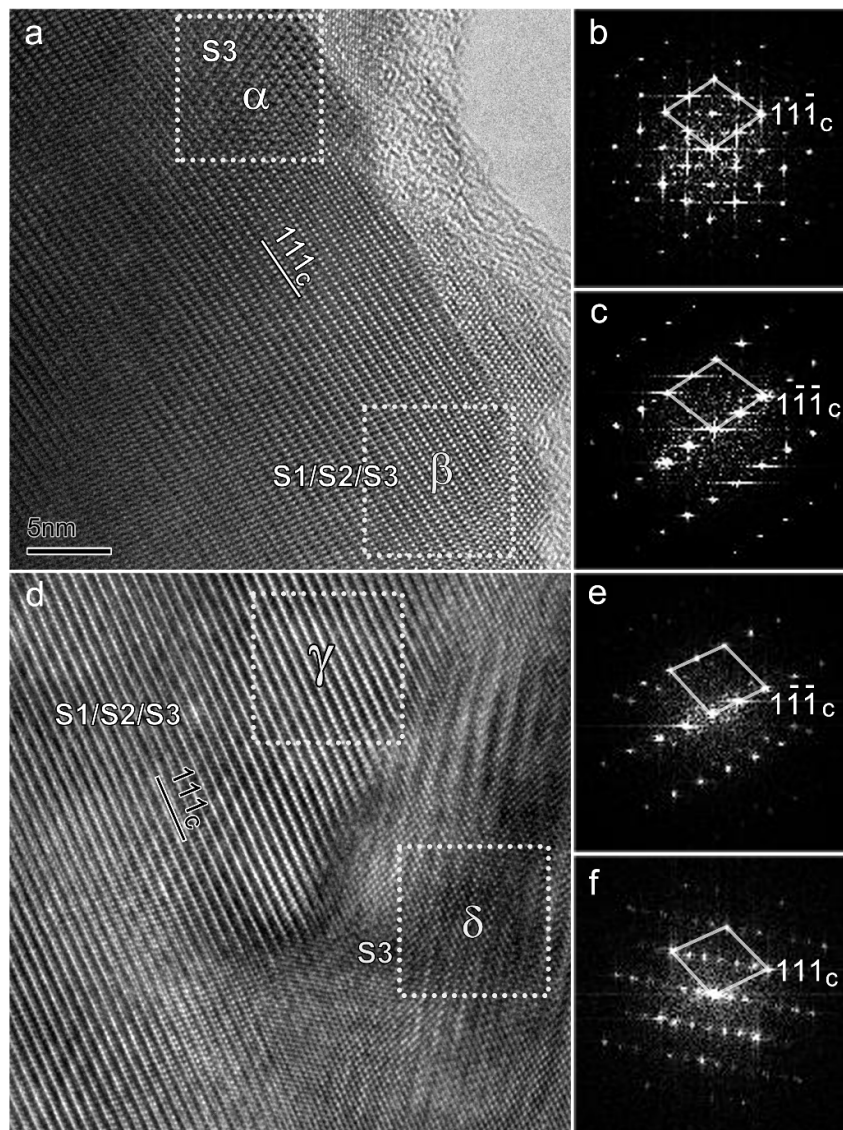


Figure 3. Lattice coherency among different phases: (a) is the high-resolution TEM image (HRTEM) of a small region in the powder sample. (b) and (c) are the fast-Fourier transformed (FFT) patterns of area α and β in (a), respectively. (d) is the lattice image of another region. (e) and (f) are FFT patterns of area γ and δ in (d), respectively. FFT patterns illustrate that different phase structures have the identical *fcc* sublattice (see frames in FFT patterns), indicative of high lattice coherency. Detailed description is presented in the text.

Structural Fluctuations during Phase Transitions

Theoretical calculation has demonstrated a smooth change in energy without any barriers during the phase transformation, a behavior typical of the second order phase transition.⁷ Here, the exact modulation of structures during heating has been examined by using *in-situ* TEM. A number of *in-situ* TEM experiments have found that the transformation temperature varies for different area in the specimen probably due to the change in local composition and internal stress. Owing to the lower energy of S3 structure than that of S1 and S2 structure, reflections peculiar to S3 are usually the first to disappear (see Fig. S4 in the supporting information). Besides, the diffraction pattern never stops changing upon increasing the temperature to that approaches the phase transition (see Fig. 4). Reflections from ordered arrangement of interlayer Cu (arrowed rows) keep altering in which some reflections disappear and reappear while some new reflections occur accompanied by variation in reflection intensities and configurations. Unfortunately, none of these newly formed ordered structures can be identified using known α -structures. What is certain is that ordered structures of interlayer Cu keep multiformity and retain the in-plane tripled superlattices though atomic configurations vary continuously.

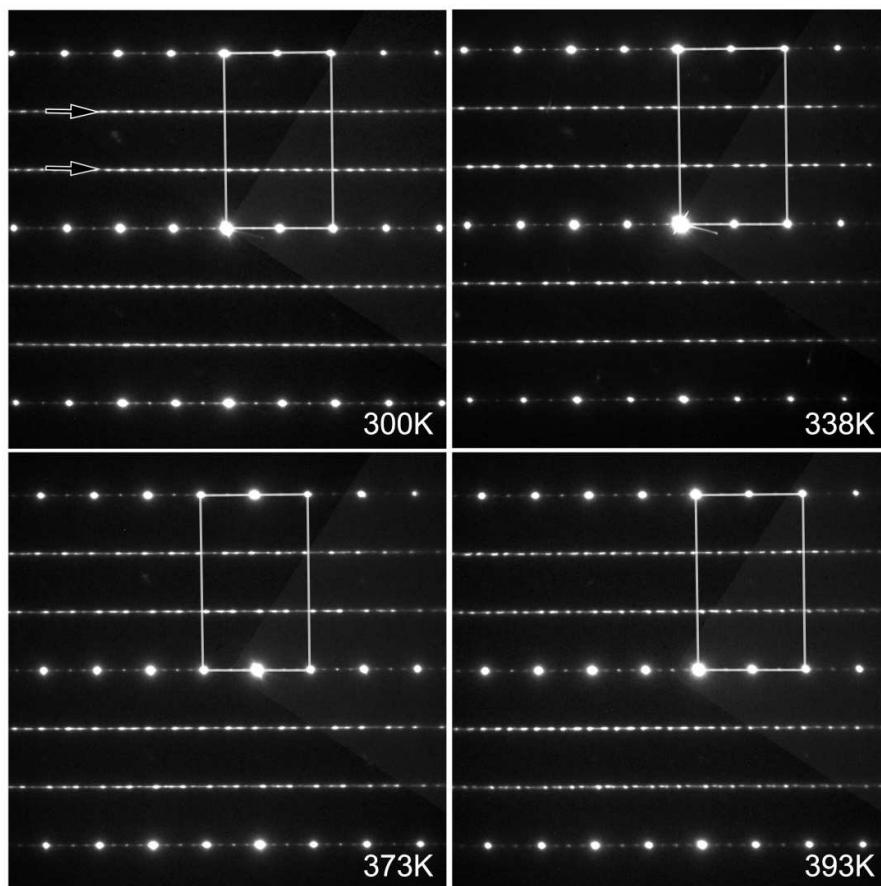


Figure 4. Evolution of diffraction patterns showing successive changes of ordered structures during heating.

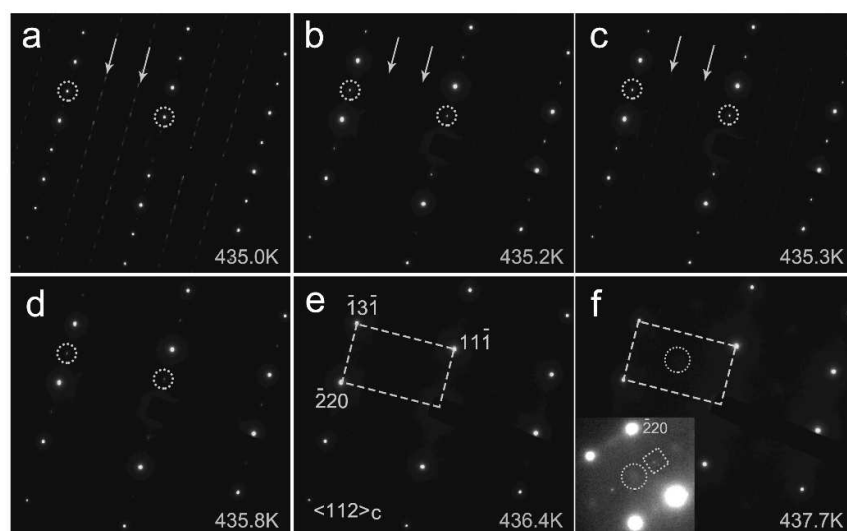


Figure 5. Evolution of diffraction patterns in an *in-situ* TEM observation during heating: The images are video clips at elevating temperatures, i.e. (a) 435.0K, (b) 435.2K, (c) 435.3K, (d) 435.8K, (e) 436.4K and (f) 437.7K. Sustained and drastic structural changes take place at

temperatures close to that for the second-order phase transition including partial disordering for Cu atoms in the interlayers (fading of arrowed reflections in (a) and (b)), oscillation of Cu order-disorder transition (intensity vibration for arrowed reflections in (b), (c) and (d)), diffusion of Cu atoms through interlayers (complete disappearance of arrowed reflections while circled reflections retain in (d)), and random distribution of Cu atoms in *fcc* crystal lattice, i.e. termination of phase transition (e). Further heating unexpectedly results in appearance of extra reflections ((f) and the inset therein) suggesting partial and short-range ordering of Cu in *fcc* lattice.

When the temperature reaches close to that for the α -to- β phase transition (see Fig. 5), the structure tends to change more frequently and drastically. First, the arrayed reflections (marked by pair of arrows in Fig. 5a and b) start to weaken, indicative of onset of disordering for interlayer Cu atoms. An interesting phenomenon illustrates that the order-disorder transition could be reversed instantly. Within a narrow temperature range, the arrayed reflections re-strengthen and then disappear immediately (see Fig. 5c and d). Fluctuation of ordered structures during heating process has been frequently observed in the present study (see Fig. S5). Thus it can be considered that diffusion of Cu atoms undergoes quite easily without any energy barrier at the critical state near the second-order phase transition. A slight oscillation in thermodynamics may result in switch in-between order and disorder or among different ordered structures (see above in Fig. 4).

When the arrayed reflections completely disappear, reflections (marked by circles in Fig. 5a-d) characteristic of layered structure still remain but decrease in intensity (see Fig. 5d). At this stage, the copper atoms are totally disordered whereas the structure still keeps the layer-type though the decreased intensity suggests parts of Cu atoms having moved to the neighboring interlayers. Upon further increasing the temperature, reflections typical of layered structures completely disappear, leaving a simple and pure diffraction pattern of high temperature cubic β -phase (see Fig. 5e). This seems the end of α -to- β phase transition in which Cu atoms have randomly but evenly occupied the $8c$ and $32f$ sites in *fcc* crystal structure. However immediately afterwards, diffused reflections appear at the center of rectangle reciprocal lattice indicating a short-range ordering of Cu in the *fcc* lattice (see Fig. 5f). Moreover,

diffraction pattern acquired using longer exposure time also reveals weak reflections at $\{110\}$ reciprocal sites (see inset in Fig. 5f). Therefore, a variety of ordered structures even exist in the high temperature phase.

Cu_2Se used to be considered as a fast ionic conductor.³¹ This is owing to the existence of large numbers of possible interstitial sites in the crystal lattice of which only 20% are occupied by Cu atoms. Therefore, the structure provides a variety of fashions for Cu ordering and pathways for Cu diffusing, which consequently results in multiformity of ordered structures and dramatic fluctuation of structures at high temperatures, respectively. The second-order phase transition of Cu_2Se illustrates extreme mobility of Cu atoms inside the comparatively steady Se cubic sublattice and involves sequential processes including formation of new ordered structures stabilized at elevated temperatures, oscillation of different ordered structures, disordering and diffusion of Cu atoms across the interlayers, and finally random distribution of Cu in a high temperature anti-fluorite cubic structure.

II. Thermal and electrical transport properties

Thermal transports

Due to the similar formation energies in several room-temperature lamellar structures, different ordered structures and their derived superperiodic structures coexist forming considerable amounts of domain boundaries. Such specific microstructures can lead to ultrastrong phonon scattering and thus low thermal conductivity. As shown in Fig. 6, the lattice thermal conductivity of Cu_2Se is reduced to around $0.28 \text{ W m}^{-1} \text{ K}^{-1}$ at 300 K. Compared to other classic thermoelectric materials such as Bi_2Te_3 , PbTe , CoSb_3 *et al.*, Cu_2Se demonstrates extremely low lattice thermal conductivity (see Fig. 6a), indicative of very short phonon mean free path. Fig. 6b summarizes the room temperature lattice thermal conductivity and phonon mean free path for several typical thermoelectric materials. The phonon mean free path of Cu_2Se is calculated based on phonon gas dynamical model,

$$\kappa_L = \frac{1}{3} C_V v l$$

where C_V is the heat capacity per volume, v is the average sound velocity, and l is the phonon mean free path (MFP). The heat capacity and the average sound velocity of typical thermoelectric materials are presented in Table S3. In the literatures,³²⁻⁴¹ the phonon MFPs of CoSb_3 and $\text{Ba}_8\text{Ga}_{16}\text{Ge}_{30}$ are around 4~5 Å at 300 K and the κ_L is between 5 and 8 $\text{W m}^{-1}\text{K}^{-1}$, while the MFPs of Bi_2Te_3 and In_4Se_3 are around 2 Å at 300 K with a κ_L of around 1 $\text{W m}^{-1}\text{K}^{-1}$. Thus, Cu_2Se shows the minimum phonon mean free path of around 1.5 Å at 300 K with a κ_L around 0.3 $\text{W m}^{-1}\text{K}^{-1}$. The present structural characterization clearly visualizes multiformity of Cu ordering, resulting in the formation of extremely large amount of boundaries or interfaces that diminish the long range phonon transfer, hence the untralow phonon MFP and κ_L .

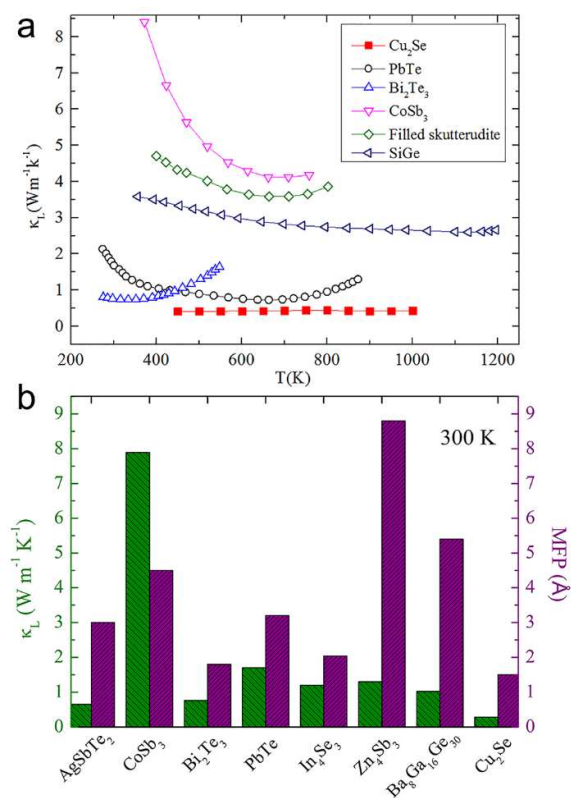


Figure 6. (a) Temperature dependence of lattice thermal conductivity for Cu_2Se as well as other typical thermoelectric materials.³² (b) Room-temperature lattice thermal conductivity in typical thermoelectric materials.³²⁻³⁹

Electrical transports

Despite of multiformity of Cu ordering, all these Cu sublattices are embedded in a uniform pseudo-cubic Se sublattice. This interesting self-independent binary-sublattice construction provides pathways for electron transfer with large carrier mobilities. In semiconductors, the mobility μ is defined as $\mu=e\tau/m$, in which e is the charge quantity, τ is the relaxation time, and m is electron effect mass. The relaxation time can be calculated based on the measured electrical resistivity (ρ) and carrier concentrations (p) $\tau= m/\rho p e^2$. The low temperature electrical resistivity and calculated carrier mobility of Cu₂Se are shown in Fig. 7a. The ρ is on the order of 10^{-6} $\Omega\cdot\text{m}$ and the μ is between 20-40 $\text{cm}^2\text{V}^{-1}\text{s}^{-1}$. These values are comparable to other typical thermoelectric materials (see Fig. 7b).⁴²⁻⁴⁹ Although the multiformity of Cu ordering as well as considerable number of interfaces and boundaries can provide additional scattering to charge carriers so as to reduce the relaxation time as well as carrier mobility, the electrical transport data suggest that large carrier mobilities are still available comparable to other semiconducting thermoelectric materials due to the well-maintained Se sublattice. By combining the almost unchanged rigid Se sublattice with the complex of Cu ordering, the lattice phonons are extremely scattered while the charge carriers are much less affected.

The current study from the microscopic point of view thus provide direct evidences to correlate the very high thermoelectric performance in Cu₂Se to its specific microstructures which contribute to both extremely low lattice thermal conductivity and good carrier mobilities. The sustained severe variation in structures during the second-order phase transition involving active movement of Cu atoms and oscillation of structural changes further intensifies scattering of electrons and phonons. However, small changes in Se sublattice during phase transition preserve a moderate carrier mobility at elevating temperatures. Overall, these structural effects eventually give rise to a rapid enhancement of thermoelectric performance up to $zT=2.3$ near the phase transition.

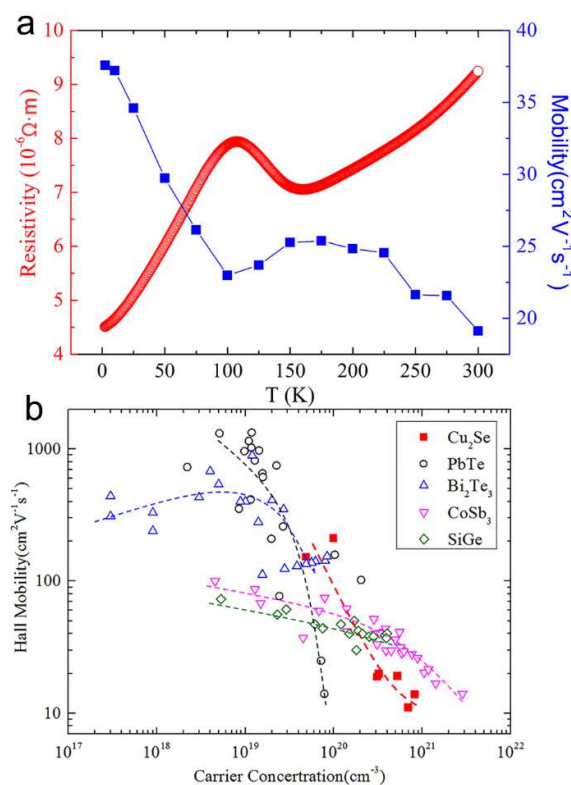


Figure 7. (a) Temperature dependence of electrical resistivity and carrier mobility for Cu₂Se. (b) Carrier mobility as a function of carrier concentration for Cu₂Se as well as a few typical thermoelectric materials.^{13,28–30,34,42–49}

Conclusions

The present structural characterizations have revealed specific self-independent binary-sublattice for Cu and Se, respectively in Cu₂Se. At room temperatures, Cu atoms congregate alternately into Se interlayers and bear an ordered configuration for energy consideration. Ordering of Cu employs variety of fashions with little energy difference, forming multiformity of Cu ordering embedded in the extensive and unique Se *fcc* sublattice. Therefore, the structure consists in microscale of large number of domains of several nanometers but in a highly coherent fashion. Such specific hybrid structures enhance the phonon scattering by polymorphic Cu ordering and domain boundaries while still guarantee good carrier mobilities due to the overall coherent lattices, which well annotate the measured extremely low thermal conductivity and well-maintained electrical transport.

The ordered structure is found to be severely fluctuated upon heating especially when the temperature approaches to the phase transition. Up there dramatic structural changes take place successively including varying of ordered structures, disordering of Cu arrangement within the interlayers, diffusing of Cu atoms across the interlayers, and finally achieving a totally random distribution of Cu in the Se cubic sublattice which has changed little during the phase transition. Meanwhile, these processes may be reversed instantly, showing oscillation of structural changes at the non-energy barrier critical states near the second-order phase transition. All these specific features strongly improve the scattering of electrons and phonons, and eventually give rise to a sudden extraordinary increase in thermoelectric performance in the close vicinity of phase transition with zT value exceeding 2. The present research implies a feasible strategy for the selection or design of promising high performance thermoelectric materials that possess a second-order phase transition in a crystal structure with two or more self-independent sublattices and sufficient interstitial sites or vacancies for an easy atomic diffusion.

Acknowledgements

This work is supported by National Natural Science Foundation of China (NSFC) under the No. 51272270, 51472262 and 61327811; National Basic Research Program of China (973-program) under Project No. 2013CB632501; the Key Research Program of Chinese Academy of Sciences (No. KGZD-EW-T06); the CAS/SAFEA International Partnership Program for Creative Research Teams; Shanghai Technical Platform for Testing and Characterization on Inorganic Materials (14DZ2292900); and Key Innovation Foundation of SICCAS.

References

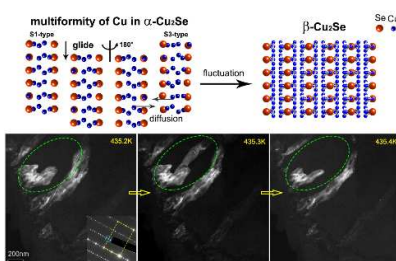
1. R. R. Heikes and R. W. Ure, *Thermoelectricity: Science and engineering*, Interscience Publishers, New York, 1961, vol. 2.

2. G. S. Nolas, J. Sharp, and J. Goldsmid, *thermoelectrics: basic principles and new materials developments*, Springer, New York, 2001, vol. 84.
3. F. D. Rosi, E. F. Hockings, and N. E. Lindenblad, *RCA Rev.*, 1961, **22**, 82–121.
4. C. Wood, *Reports Prog. Phys.*, 1988, **51**, 459–539.
5. F. D. Rosi, *Solid. State. Electron.*, 1968, **11**, 833–848.
6. L. E. Bell, *Science*, 2008, **321**, 1457–1461.
7. F. J. DiSalvo, *Science*, 1999, **285**, 703–706.
8. B. Poudel, Q. Hao, Y. Ma, Y. Lan, A. Minnich, B. Yu, X. Yan, D. Wang, A. Muto, D. Vashaee, X. Chen, J. Liu, M. S. Dresselhaus, G. Chen, and Z. Ren, *Science*, 2008, **320**, 634–638.
9. K. Biswas, J. He, I. D. Blum, C.-I. Wu, T. P. Hogan, D. N. Seidman, V. P. Dravid, and M. G. Kanatzidis, *Nature*, 2012, **489**, 414–418.
10. R. Venkatasubramanian, E. Siivola, T. Colpitts, and B. O’Quinn, *Nature*, 2001, **413**, 597–602.
11. T. C. Harman, P. J. Taylor, M. P. Walsh, and B. E. LaForge, *Science*, 2002, **297**, 2229–2232.
12. Y. He, T. Day, T. Zhang, H. Liu, X. Shi, L. Chen, and G. J. Snyder, *Adv. Mater.*, 2014, **26**, 3974–3978.
13. H. Liu, X. Shi, F. Xu, L. Zhang, W. Zhang, L. Chen, Q. Li, C. Uher, T. Day, and G. J. Snyder, *Nat. Mater.*, 2012, **11**, 422–425.
14. K. Okamoto, *Jpn. J. Appl. Phys.*, 1971, **10**, 508.
15. D. R. Brown, T. Day, K. a. Borup, S. Christensen, B. B. Iversen, and G. J. Snyder, *APL Mater.*, 2013, **1**, 052107.
16. H. Liu, X. Shi, M. Kirkham, H. Wang, Q. Li, C. Uher, W. Zhang, and L. Chen, *Mater. Lett.*, 2013, **93**, 121–124.
17. H. Liu, X. Yuan, P. Lu, X. Shi, F. Xu, Y. He, Y. Tang, S. Bai, W. Zhang, L. Chen, Y. Lin, L. Shi, H. Lin, X. Gao, X. Zhang, H. Chi, and C. Uher, *Adv. Mater.*, 2013, **25**, 6607–6612.
18. B. Celustka and Z. Ogorelec, *J. Phys. Chem. Solids*, 1966, **27**, 957–960.
19. R. D. Heyding, *Can. J. Chem.*, 1966, **44**, 1233–1236.
20. M. Oliveria, R. K. McMullan, and B. J. Wuensch, *Solid State Ionics*, 1988, **30**, 1332–1337.

21. A. N. Skomorokhov, D. M. Trots, M. Knapp, N. N. Bickulova, and H. Fuess, *J. Alloys Compd.*, 2006, **421**, 64–71.
22. S. a. Danilkin, M. Avdeev, M. Sale, and T. Sakuma, *Solid State Ionics*, 2012, **225**, 190–193.
23. S. Kashida and J. Akai, *J. Phys. C Solid State Phys.*, 1988, **21**, 5329–5336.
24. Ritc. M. Murray and R. D. Heyding, *Can. J. Chem.*, 1975, **53**, 878–887.
25. R. D. Heyding and R. M. Murray, *Can. J. Chem.*, 1976, **54**, 841–848.
26. Z. Vucik, O. Milat, V. Horvatić, and Z. Ogorelec, *Phys. Rev. B*, 1981, **24**, 5398–5402.
27. M. C. Nguyen, J.-H. Choi, X. Zhao, C.-Z. Wang, Z. Zhang, and K.-M. Ho, *Phys. Rev. Lett.*, 2013, **111**, 165502.
28. X. Su, F. Fu, Y. Yan, G. Zheng, T. Liang, Q. Zhang, X. Cheng, D. Yang, H. Chi, X. Tang, Q. Zhang, and C. Uher, *Nat. Commun.*, 2014, **5**, 4908.
29. D. Li, X. Y. Qin, Y. F. Liu, C. J. Song, L. Wang, J. Zhang, H. X. Xin, G. L. Guo, T. H. Zou, G. L. Sun, B. J. Ren, and X. G. Zhu, *RSC Adv.*, 2014, **4**, 8638–8644.
30. X. Shi, J. Yang, J. R. Salvador, M. Chi, J. Y. Cho, H. Wang, S. Bai, J. Yang, W. Zhang, and L. Chen, *J. Am. Chem. Soc.*, 2011, **133**, 7837–7846.
31. T. Takahashi, O. Yamamoto, F. Matsuyama, and Y. Noda, *J. Solid State Chem.*, 1976, **16**, 35–39.
32. G. J. Snyder and E. S. Toberer, *Nat. Mater.*, 2008, **7**, 105–114.
33. D. Morelli, V. Jovovic, and J. Heremans, *Phys. Rev. Lett.*, 2008, **101**, 035901.
34. T. Caillat, A. Borshchevsky, and J. P. Fleurial, *J. Appl. Phys.*, 1996, **80**, 4442–4449.
35. S. Bhattacharya, R. Hermann, V. Keppens, T. Tritt, and G. Snyder, *Phys. Rev. B*, 2006, **74**, 134108.
36. M. Christensen, A. B. Abrahamsen, N. B. Christensen, F. Juranyi, N. H. Andersen, K. Lefmann, J. Andreasson, C. R. H. Bahl, and B. B. Iversen, *Nat. Mater.*, 2008, **7**, 811–815.
37. J. P. Heremans, V. Jovovic, E. S. Toberer, A. Saramat, K. Kurosaki, A. Charoenphakdee, S. Yamanaka, and G. J. Snyder, *Science*, 2008, **321**, 554–557.
38. J.-S. Rhyee, E. Cho, K. H. Lee, S. M. Lee, S. Il Kim, H.-S. Kim, Y. S. Kwon, and S. J. Kim, *Appl. Phys. Lett.*, 2009, **95**, 212106.
39. B. Y. Yavorsky, N. F. Hinsche, I. Mertig, and P. Zahn, *Phys. Rev. B*, 2011, **84**, 165208.

40. X. Chen, D. Parker, and D. J. Singh, *Phys. Rev. B*, 2013, **87**, 045317.
41. J. Dadda, E. Müller, S. Perlt, T. Höche, P. B. Pereira, and R. P. Hermann, *J. Mater. Res.*, 2011, **26**, 1800–1812.
42. H. Chi, H. Kim, J. C. Thomas, G. Shi, K. Sun, M. Abeykoon, E. S. Bozin, X. Shi, Q. Li, X. Shi, E. Kioupakis, A. Van der Ven, M. Kaviani, and C. Uher, *Phys. Rev. B*, 2014, **89**, 195209.
43. B. Abeles, D. Beers, G. Cody, and J. Dismukes, *Phys. Rev.*, 1962, **125**, 44–46.
44. K. Favier, G. Bernard-Granger, C. Navone, M. Soulier, M. Boidot, J. Leforestier, J. Simon, J.-C. Tedenac, and D. Ravot, *Acta Mater.*, 2014, **64**, 429–442.
45. J. P. Heremans, C. M. Thrush, and D. T. Morelli, *J. Appl. Phys.*, 2005, **98**, 063703.
46. J. Jiang, L. Chen, S. Bai, Q. Yao, and Q. Wang, *Mater. Sci. Eng. B*, 2005, **117**, 334–338.
47. C. Satterthwaite and R. Ure, *Phys. Rev.*, 1957, **108**, 1164–1170.
48. H. J. Wu, L.-D. Zhao, F. S. Zheng, D. Wu, Y. L. Pei, X. Tong, M. G. Kanatzidis, and J. Q. He, *Nat. Commun.*, 2014, **5**, 4515.
49. L.-D. Zhao, B.-P. Zhang, W.-S. Liu, and J.-F. Li, *J. Appl. Phys.*, 2009, **105**, 023704.

TOC



Ultra-low thermal conductivity arisen from multiformity and fluctuation of Cu ordering in Cu_2Se thermoelectric materials.